Crystallization kinetics of mullite from single-phase gel determined by isothermal differential scanning calorimetry

E. Tkalcec [a,*], R. Nass [a], J. Schmauch [b], H. Schmidt [a], S. Kurajica [c], A. Bezjak [c], H. Ivankovic [c]

[a] *Institut für Neue Materialien, Im Stadtwald, Gebäude 43, 66123 Saarbrücken, Germany*
[b] *Universität des Saarlandes, Fachbereich 10.3 Technische Physik, Im Stadtwald, Gebäude 43B, 66123 Saarbrücken, Germany*
[c] *Faculty of chemical Engineering and Technology, University of Zagreb, 10000 Zagreb, Croatia*

Received 20 November 1996; revised 18 August 1997

Abstract

Transformation kinetics of single-phase gel with mullite composition was studied by isothermal differential calorimetry (DSC) in temperature range from 937 to 959°C. Single exotherm was observed for annealing temperatures below 947°C, and two overlapped exothermic peaks were seen above this temperature. According to XRD analysis, mullite was the only phase crystallized either under non-isothermal or isothermal heat treatment. Johnson–Mehl–Avrami (JMA) equation for nucleation and growth could not describe mullite crystallization adequately, even below 947°C. Using bimodal JMA-type model, that proposes mullite crystallization in two steps, the fitting was remarkably good in the whole temperature range. Obtained kinetics data do not allow one to characterize the gel, either as typical single phase one (nucleation-controlled process with two rate constants and small apparent activation energies), or as hybrid gel (mullite formation via spinel and high apparent activation energies). The rate constants were an order of magnitude smaller than is proposed for single phase gel. The apparent activation energies, however ($E_{a1} = 1053 \pm 51$ kJ/mol, and $E_{a2} = 1028 \pm 22$ kJ/mol), were in great discrepancy to those already cited for single phase gels, but they were in very good agreement with data evaluated for diphasic and hybrid gels. Mullite *a*-axis length and effective fraction of mullite that is formed in the first and second step of the process provided an insight in the mechanism of mullite crystallization. It is assumed that not the nucleation and crystallization limitations, rather the phase separation is the controlling process in mullite formation from single phase gel under applied experimental conditions.

1. Introduction

Requirement for high purity, homogeneity and density of mullite lead to the consideration of sol–gel fabrication of mullite powders. Diverse starting materials and synthesis methods were studied for preparation of mullite precursors [1–4]. Transformation pathways of mullite precursors are generally grouped in three types. Single-phase precursors in which silica and alumina are dispersed at atomic to molecular levels show direct mullite crystallization at about

* Corresponding author. Tel.: +49-681 302 5248; fax: +49-681 302 5242; e-mail: tkalcec@inm.uni-sb.de.

980°C. Colloidal and hybrid gels show spinel formation at similar temperatures with mullite formation at about 1200°C. In diphasic gels, boehmite or other transition alumina and silica exist to > 1250°C, and upon further heating they form mullite.

Precursors derived from aluminium nitrate nonahydrate (ANN) and TEOS form no aluminosilicate complexes during gelation [5], nevertheless intimate mixing was achieved by trapping of ANN solution in the silica gel network. Crystallization of mullite from single-phase gels occurs by nucleation controlled process [6], whereas in diphasic gels either interface-controlled or near-interface-diffusion controlled crystallization occurs [7,8]. Huling and Messing [9] emphasized that many gel systems claimed to be single-phase are in reality diphasic, and crystallization of mullite at 980°C is due to phase separation. Crystallization processes are crucial in achieving good mechanical properties, therefore, it is very important to understand crystallization mechanisms of amorphous single-phase mullite precursors.

Li and Thomson [10] employed non-isothermal DTA to study mullite crystallization from diphasic gels. To the best of our knowledge, there are no data concerning crystallization of single-phase mullite gels measured by isothermal DSC.

The aim of this study was detailed examination of crystallization mechanism in amorphous premullite single-phase xerogels derived from aluminium nitrate nonahydrate (ANN) and tetraethoxysilane (TEOS).

2. Experimental procedure

Gel with Al/Si = 3/1 was prepared by using tetraethoxysilane (TEOS) > 98% and aluminium nitrate nonahydrate (ANN). Aluminium nitrate nonahydrate was dissolved in absolute ethanol by stirring for 24 h at 60°C. The molar ratio of Al/ethanol was 1/9. TEOS previously mixed with ethanol (TEOS/EtOH = 1:9) was added dropwise to ANN solution under vigorous stirring. The batch solution was refluxed at 60°C until gelation. The gel was dried in vacuum at 60°C and milled using agate balls. To prevent structural changes of dried powder due to humidity, as-dried gel was divided into portions and stored in a desiccator.

Isothermal differential scanning calorimetry was carried out by a DSC (Netzsch Model 404) between 937 and 959°C in air. 30 ± 0.5 mg of dried gel was put in a Pt pan, while an empty pan was used as standard. As-dried gel was heated at 30 K/min and held isothermally for 2 h. DSC apparatus temperature calibration was carried out for different heating rates employing high purity materials approved by ICTA (Ag_2SO_4, quartz, K_2SO_4 and $BaCO_3$) according to [11]. The overall temperature accuracy of the instrument is expected to be within ± 0.5 K. The transition temperature of $BaCO_3$ was also checked from time to time in between the carrying out the experiments. DSC was calibrated for enthalpy between 800 and 1000°C by measuring the heat capacity of sapphire using C_ps from the literature. Enthalpy accuracy measurement was determined to be within $\pm 5\%$ by measuring the heat capacity of palladium between 800 and 1050°C. Crystallization enthalpy of mullite was determined from the area of a DSC peak at the heating rate of 20 K/min. During the DSC experiment an as-prepared gel loses about half of its weight, hence the sample was also weighed after analysis and this weight was used for the evaluation of the crystallization enthalpy.

Simultaneous differential thermal analysis (DTA), thermogravimetry (TG) and evolved gas analysis (EGA) measurements were performed under a constant oxygen flow of 75 cm^3/min, using a thermoanalyser (Netzsch STA/QMS 409/429-403), connected with quadrupole mass spectrometer (Balzers QMG 420, 1–200 m/z). The gas analysis was performed in steps of 10 K. One hundred thirty mg of the sample in an Al_2O_3 sample holder were analyzed.

At the end of each DSC or DTA/TG/MS experiment, the sample was quenched and analysed by X-ray diffraction. X-ray diffraction analysis (XRD) was carried out on a computer controlled diffractometer (Siemens D500/PSD) using Cu Kα radiation, a quartz single-crystal monochromator, and a curved position sensitive detector. Samples were dispersed on a Si single crystal holder. Data were collected in step scan mode between 5 and 70° 2θ with steps of 0.02° and counting time of 10 s per step. Mullite lattice constants were determined by the

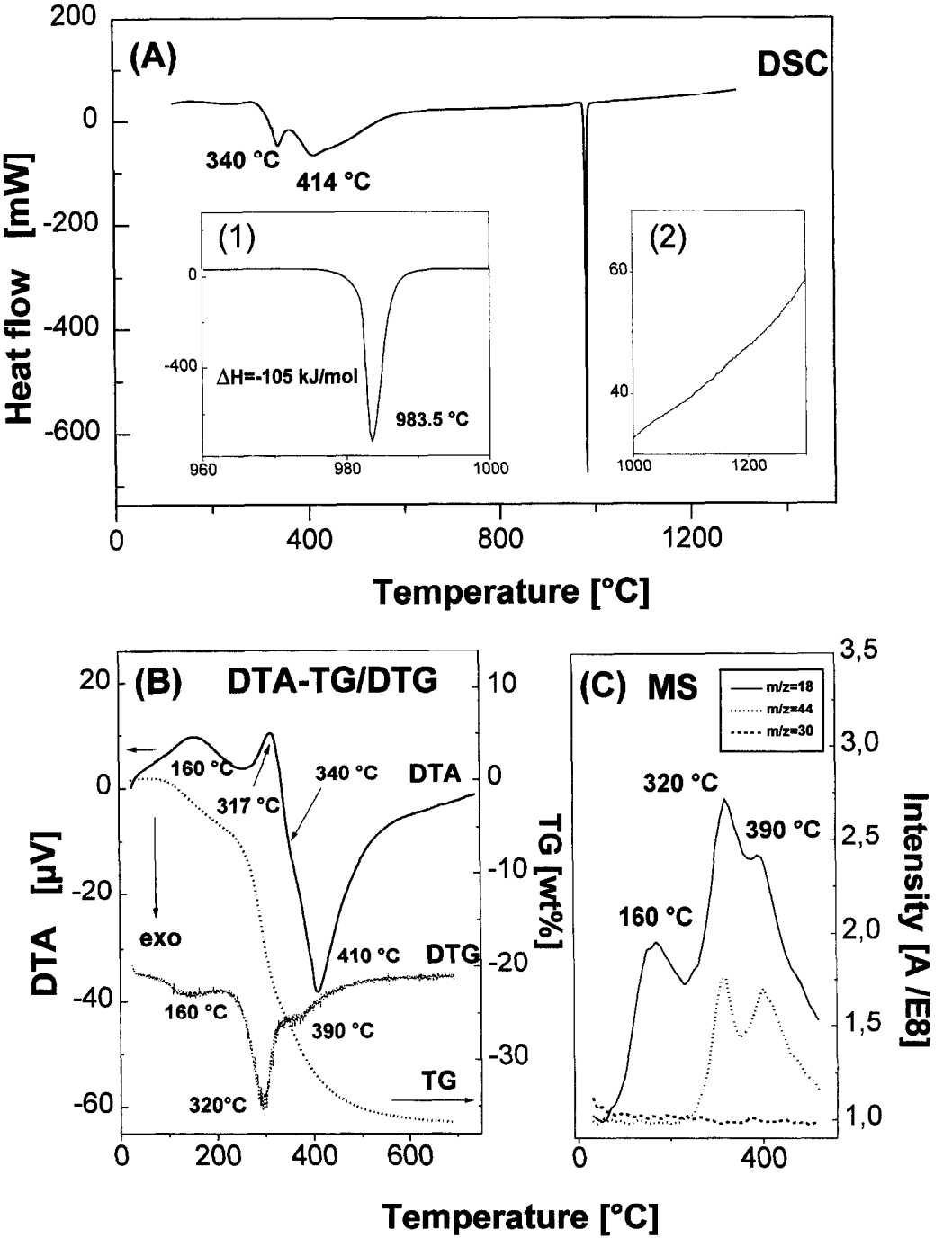

Fig. 1. (A) DSC scan of as-dried gel at the heating rate of 20 K min^{-1}, (1) = DSC scan in the temperature range from 960 to 1000°C, (2) = enlarged view of DSC in the range from 1000 to 1300°C. (B) Simultaneous DTA and TG/DTG curves of the same gel heated up to 700°C. (C) Corresponding mass spectra of gases evolved during heating in flowing oxygen.

Rietveld refining method [12,13]. Alumina content in mullite was calculated from the relation between lattice constant a and mullite composition [14], and the crystallite size was determined by Scherrer method [15] using 13 strong lines in a diffraction angle interval of 30–70° 2θ.

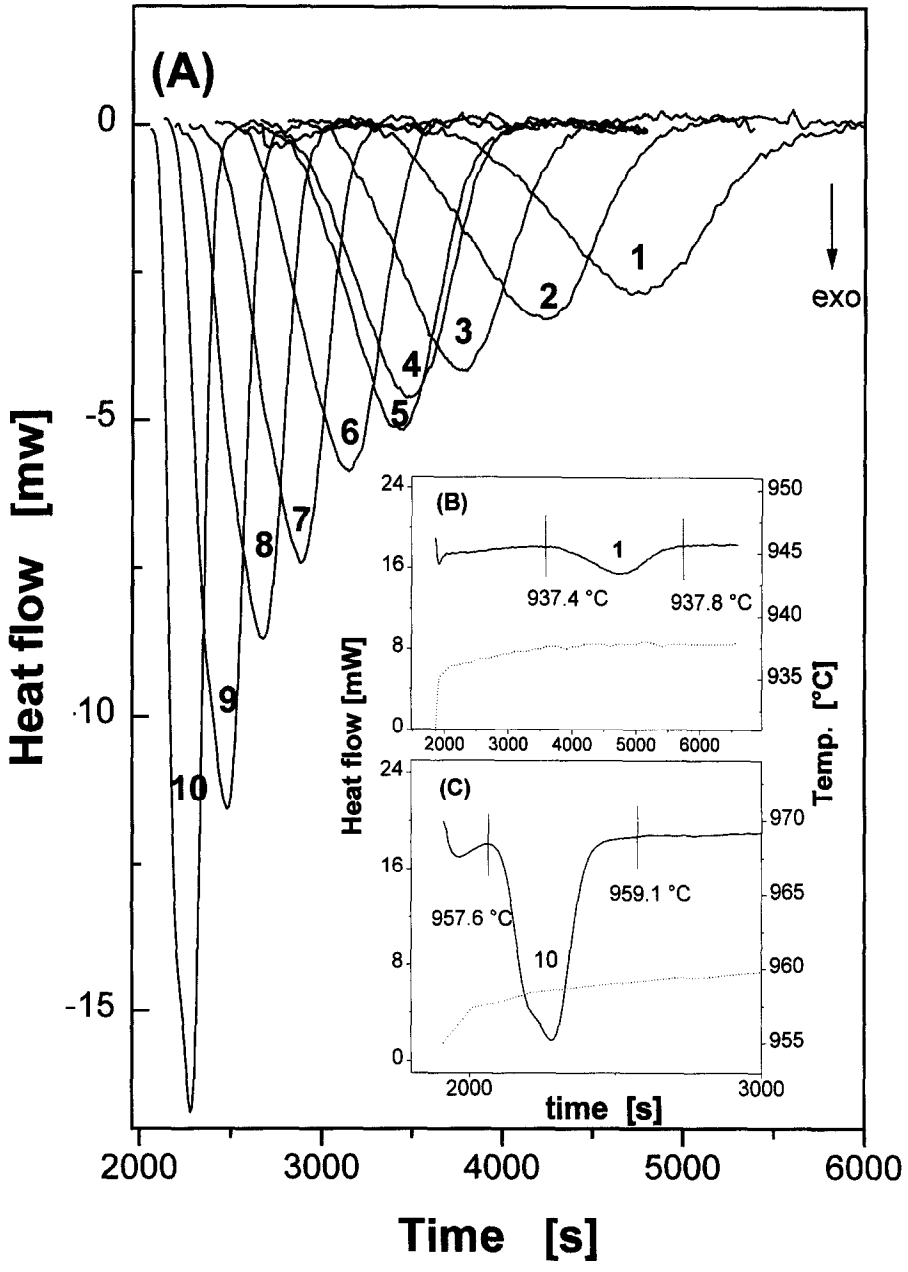

Fig. 2. (A) Isothermal DSC scans at various annealing temperatures. 1 = 938°C, 2 = 940°C, 3 = 942°C, 4 = 944°C, 5 = 945°C, 6 = 947°C, 7 = 949°C, 8 = 951°C, 9 = 954°C, 10 = 959°C. (B) Enlarged view of isothermal DSC curve at annealing temperature of 938°C (sample No. 1), showing temperature fluctuation during DSC analysis. The mean temperature value recorded during the time of mullite crystallization is expressed as annealing temperature. (C) Enlarged view of isothermal DSC curve at 959°C and temperature fluctuation during annealing.

3. Results

The DSC scan of as-dried gel at the heating rate of 20 K min^{-1} is shown in Fig. 1A. According to Ban et al. [16], the peaks in the low temperature range are caused by dehydration, dehydroxylation and decomposition of nitrates and alkoxydes. Since the processes are mutually interdependent and overlapped, a proper assignation of peaks seen in DSC scan can be obtained only by simultaneous DSC/TG (or DTA/TG) analysis combined with EGA. The results of DTA, TG/DTG (derivative TG) and EGA are given in Fig. 1B and C. In TG scan (Fig. 1B), a three-step weight decrease is observed. The first step at 160°C corresponds entirely to endothermic effect in DTA scan. The second step occurs at 320°C, but its endothermic magnitude is less obvious in DTA curve, since it is partially overlapped by an exothermic effect. The endothermic third weight loss at about 390°C is invisible in DTA scan, since in the same temperature range a strong exotherm occurs with maximum at 410°C. At the lower temperature side of the exothermic peak, a small just visible shoulder (at about 340°C) can be noticed. Mass spectra of evolved gases are given in Fig. 1C. Three peaks in the mass signal for H_2O ($m/z = 18$), at 160, 320 and 390°C, match the weight loss steps in the TG data, and two of them (at 320 and 390°C) coincide with peaks in the mass signal for CO_2 ($m/z = 44$). That suggests that the evolution of molecular water is dominant at 160°C, whereas dehydroxylation and decomposition of organics occur in two steps, at 320 and 390°C. It was not possible to determine any peak in the mass signal of nitrates ($m/z = 30$), since nitrogen impurity in oxygen surpasses the amount of NO_2 gas evolved from the gel. That can be explained by vacuum drying of the gel. An exothermic peak in DTA scan at 410°C with a small barely visible shoulder at about 340°C has to be attributed to the combustion of organics. In comparison to DTA, the DSC scan showed two well-resolved peaks, at 340 and 414°C. This difference has to be attributed to greater sensitivity of DSC method. Contrary to the results given by Ban et al. [16], both endothermic and exothermic effects were observed in DSC/DTA data. We assume that hydrolyzable ($-OC_2H_5$) groups predominate in our sample. In Fig. 1A, inset (1), the segment of the DSC in the temperature range between 960 and 1000°C is shown. An exotherm at 983.5°C is attributed either to the formation of mullite, or spinel, or both. When spinel crystallizes at ~ 980°C, the peak is smaller [4] and at 1250°C a small exotherm is also generally recorded [4,17]. The segment of the same DSC scan between 1000 and 1300°C (recorded with greater sensitivity), given in inset (2) of Fig. 1A, shows that there is no evidence for spinel formation at 980°C. XRD analysis of the sample quenched in DSC from 1000°C (not presented) provided additional evidence that no spinel was formed simultaneously with mullite at 980°C. The crystallization enthalpy determined from the peak area at 980°C, yields $(\Delta H)_c = -105$ kJ mol^{-1}, which is in good agreement with the result of $(\Delta H)_c = -106$ kJ mol^{-1} reported by Sen and Thiagarajan [18] for single phase xerogel.

Isothermal DSC data obtained at 10 different annealing temperatures over the range from 937 to 959°C are shown in Fig. 2A. To check the reproducibility of measurements a sample was analyzed three times at one and the same annealing temperature. The reproducibility of the annealing temperature was found to be within ± 0.5 K, and the enthalpy within 5%.

DSC scans in Fig. 2A can be divided into two groups. Each group is represented in detail by one DSC scan. In Fig. 2B, DSC scan at 938°C is given. It represents the first group of curves in which one exothermic peak could be observed (curves No. 1, 2, 3, 4, 5 and 6; temperature range from 938 to 947°C). Fig. 2C shows DSC scan of the sample annealed at 959°C (curve No. 10). It represents the second group of curves with two overlapping maxima (curves No. 7, 8, 9 and 10; annealing temperature above 947°C).

In the first approach, mullite crystallization below 947°C (one exothermic peak observed on DSC scan) was treated as one-rate constant process. In that case, the volume fraction transformed as a function of time, $\alpha(t)$, can be fitted to the Johnson–Mehl–Avrami (JMA) nucleation and growth kinetics model [19]. Fig. 3A shows the DSC data in an isothermal mode at 938°C and the best fit under the assumption that mullite crystallization can be described by the JMA equation. The adjustable parameters were calculated by minimizing chi-square function. Evidently, the calculated curve does not fit the experimental data well. The discrepancies between experi-

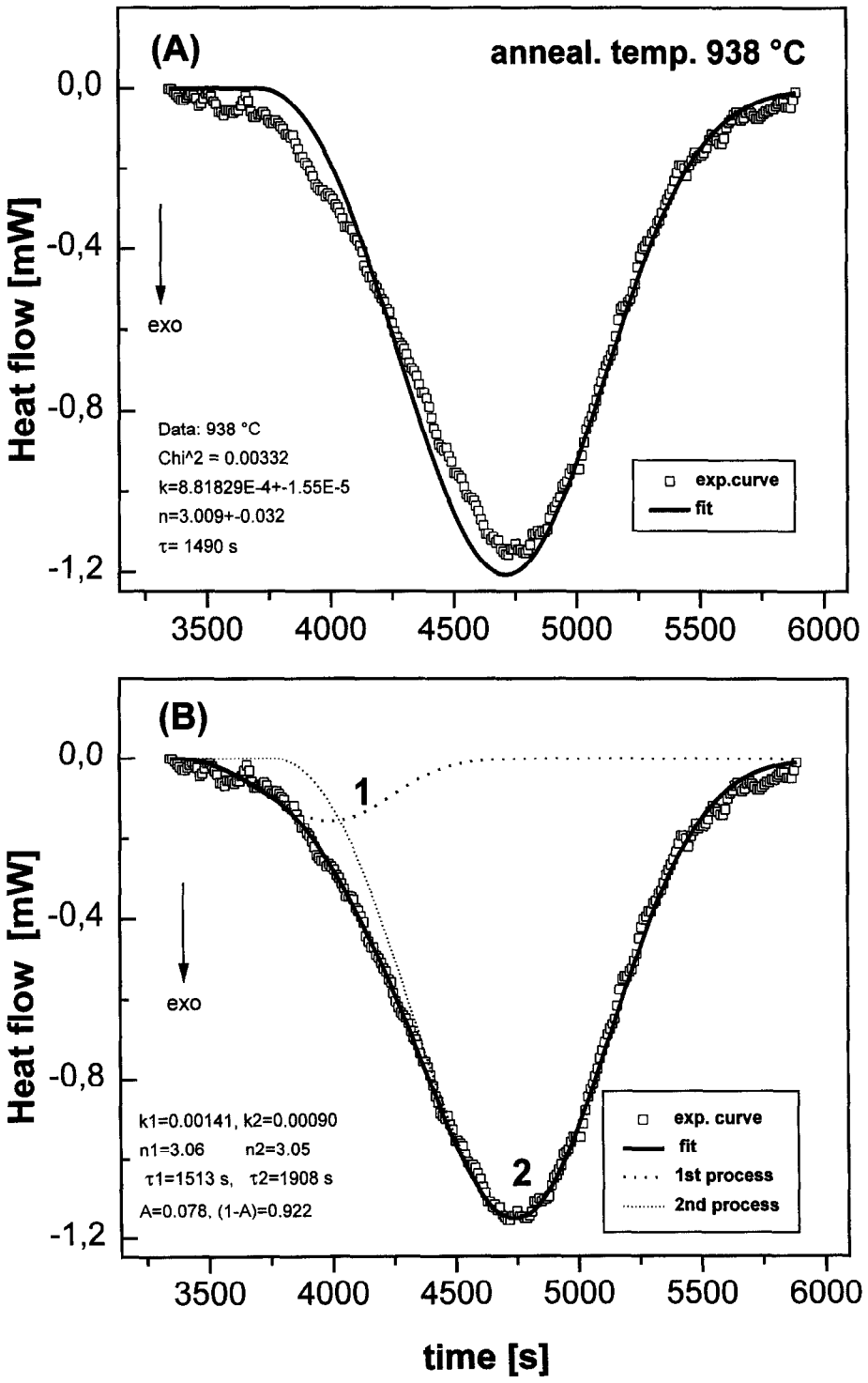

Fig. 3. Isothermal DSC scan at annealing temperature of 938°C (sample No. 1), and the fitted data under the assumption of: (A) one-step mullite formation and (B) two-step formation.

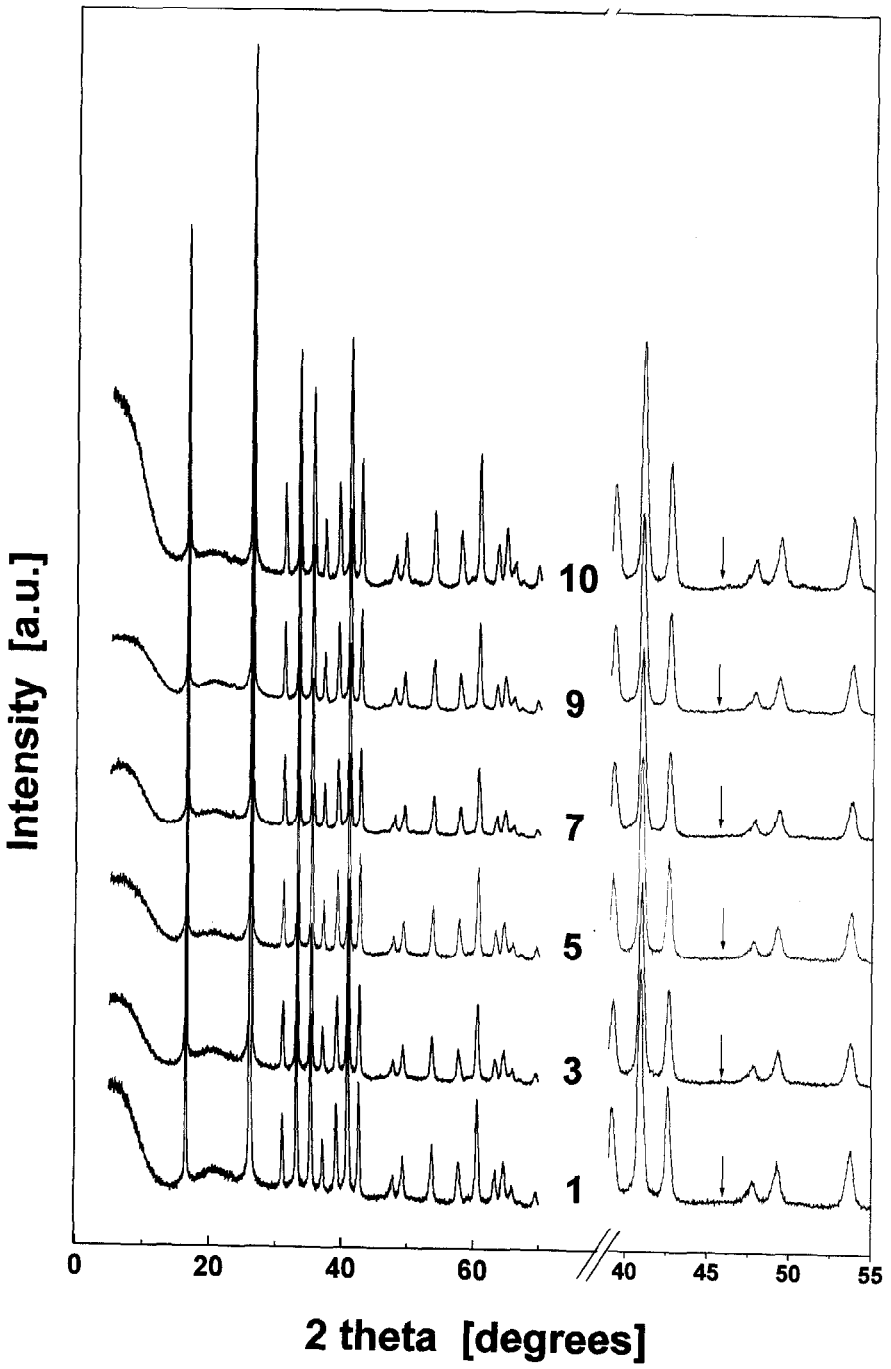

Fig. 4. XRD patterns of the samples quenched after 2 hours annealing at different temperatures. The position of 46°2θ, where the second strongest (400) spinel reflection should be noticed is marked with arrow in the left patterns. For clarity the mullite reflections are not marked. The notation of samples is the same as in Fig. 2, and in Table 1.

mental and fitted curves are even greater at higher annealing temperatures (curves No. 2, 3, 4, 5 and 6). A possible explanation for this could be simultaneous crystallization of two phases with different rate constants. However, in the XRD patterns shown in Fig. 4 only mullite was observed, even in the temperature range where two overlapped peaks are seen on DSC scans (samples No. 7, 8, 9 and 10). The positions of 46°2θ where the second strongest spinel reflection, 400, should be noticed are marked by arrows.

Studying the crystallization kinetics of mullite from single phase gels by dynamic X-ray diffraction (DXRD), Li and Thomson [6] also noticed that it was not possible to fit experimental data to an Avrami-type model with one nucleation rate. They obtained an adequate fitting only by using a model with two distinct nucleation rates. According to them a local nonuniform mixing led to an inhomogeneity among particles that can be described only by two distinct nucleation rates. Taking into consideration Li and Thomson's results, and the fact that DSC data above 947°C show two overlapped exothermic peaks (Fig. 2C), the assumption was made that mullite crystallizes in a two-step process even below 947°C. Therefore, the experimental data were fitted to the following model for two overlapping peaks:

$$\begin{aligned} d\alpha/dt = A \cdot & \left\{ \left[k_1^{n_1} n_1 (t-\tau_1)^{(n_1-1)} \right] \right. \\ & \left. \times \exp\left[-k_1^{n_1} (t-\tau_1)^{n_1} \right] \right\} \\ & + (1-A) \left\{ \left[k_2^{n_2} n_2 (t-\tau_2)^{(n_2-1)} \right] \right. \\ & \left. \times \exp\left[-k_2^{n_2} (t-\tau_2)^{n_2} \right] \right\}, \end{aligned}$$

where A is the ratio between enthalpy release attributed to the first process (first resolved peak area, see Fig. 3B) and the total enthalpy of transformation, $(\Delta H)_T$ (total peak area), whereas $(1-A)$ is the ratio between enthalpy change during the second process (second resolved peak area, Fig. 3B) and the total enthalpy of transformation $(\Delta H)_T$ at annealing temperature T. Since in both processes the same crystalline phase occurs, the crystallization of the same fraction of mullite in any of two steps is expected to be related to the same enthalpy release. In this special case, A and $(1-A)$ can have the meanings

Table 1
Calculated parameters for two-step model of mullite crystallization for different isothermal annealing temperatures

Sample No.	T [a] (°C)	$(\Delta H)_T$ [b] (kJ mol^{-1})	Kinetic parameters						
			$k_1 \times 10^3$ [c] (s^{-1})	n_1 [d]	τ_1 (s)	A	$k_2 \times 10^3$ [c] (s^{-1})	n_2 [d]	τ_2 (s)
1	938	−85	1.41	3.06	1513	0.078	0.90	3.05	1908
			0.88 [e]	3.00 [e]	1490 [e]	–	–	–	–
2	940	−91	1.46	3.43	1253	0.110	0.99	3.49	1500
3	942	−97	1.81	3.30	1005	0.098	1.18	3.47	1196
4	944	−93	1.88	3.31	826	0.154	1.41	3.46	1053
5	945	−96	2.20	3.27	858	0.124	1.46	3.48	1008
6	947	−98	2.43	3.31	680	0.197	1.84	3.35	868
7	949	−99	2.93	3.40	525	0.193	2.11	3.54	656
8	951	−100	3.74	3.53	421	0.194	2.55	3.51	517
9	954	−100	4.91	3.53	347	0.223	3.42	3.52	443
10	959	−100	8.06	3.52	269	0.212	4.77	3.65	291

$(\Delta H)_T$ = reaction enthalpy of the whole process; k_1 and k_2: rate constants; n_1 and n_2: Avrami exponents; τ_1 and τ_2; incubation times; A and $(1-A)$: mullite fraction formed in the first and the second step of the process.

[a] The overall temperature accuracy of the instrument is expected to be within ±0.5 K. The reproducibility of an annealing temperature proved by three measurements of the sample at one and the same annealing temperature was within ±0.5 K.

[b] Enthalpy accuracy measurement is within ±5%.

[c] The standard deviations of k_1 and k_2 are smaller than $\pm 8 \times 10^{-5}$.

[d] The standard deviations of n_1 and n_2 are smaller than ±0.05.

[e] Calculated using one-step model.

of mullite fractions transformed in the first and second step of the crystallization process, respectively. Computer program for peak separation and simultaneous calculation of kinetic parameters for two-step crystallization process with a small time lag, described by Kurajica et al. [20], was used.

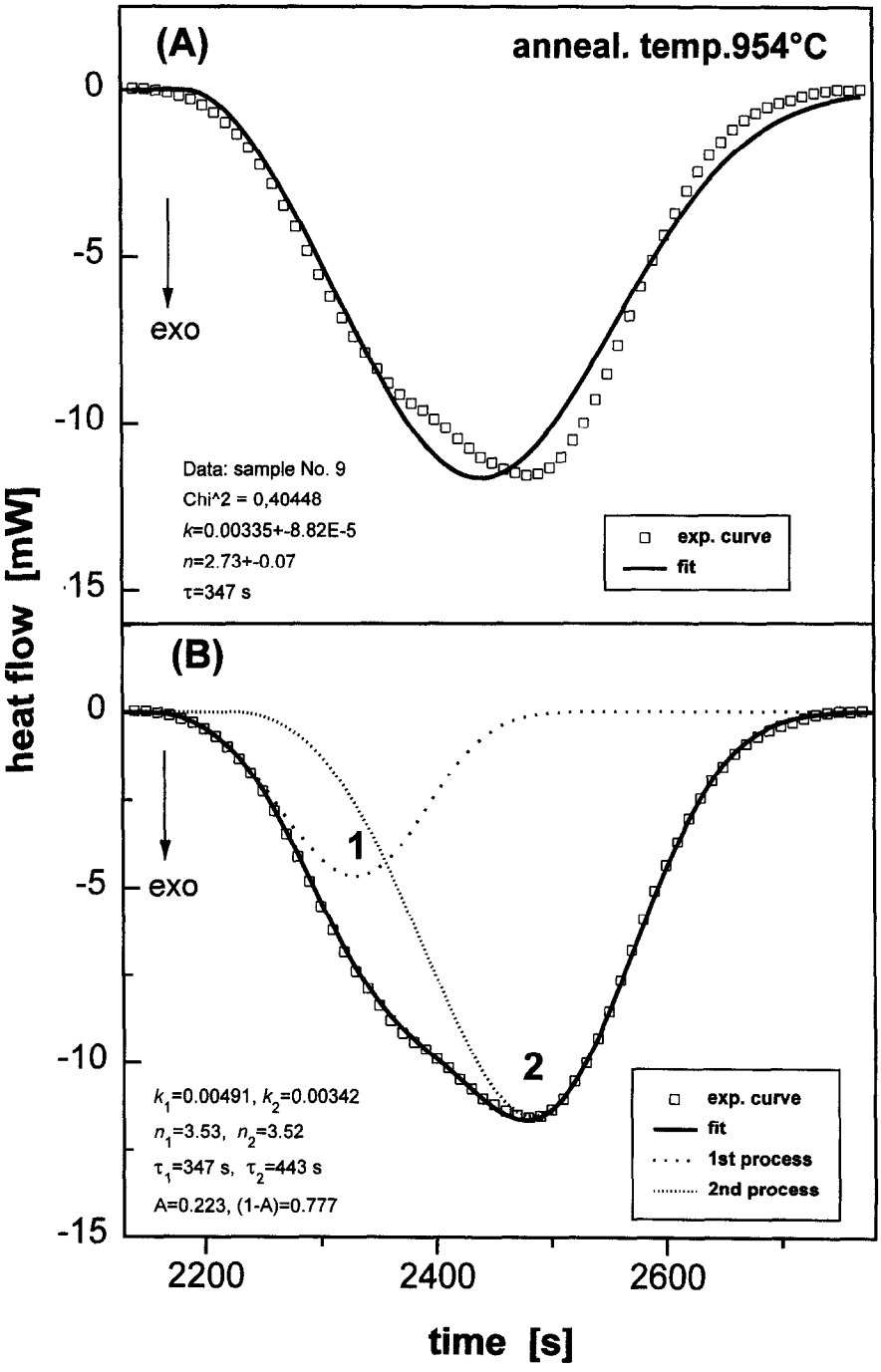

Fig. 5. Isothermal DSC curve at annealing temperature of 954°C (sample No. 9), and fitted data under the assumption of: (A) one-step mullite crystallization, and (B) two-step crystallization.

Two sets of kinetic parameters, k_1, n_1, τ_1, A, and k_2, n_2, τ_2, $(1-A)$, and two theoretical functions corresponding to different crystallization processes can be obtained. The best fitting curve (solid line) for two-step model and the resolved peaks 1 and 2 (dot lines) for sample annealed at 938°C are given in Fig. 3B. It has to be taken into account that the curves in Fig. 3A and B are plotted as a function of integral time from the beginning of heat treatment, i.e., the time needed to bring the sample to annealing temperature is also included. Kinetic parameters, calculated by using a binary model (Eq. (1)), are given in Table 1.

The same two-step model was also applied to curves No. 7, 8, 9 and 10. In Fig. 5 numerical approximations using one- and two-step model for the experimental curve No. 9 are shown. The solid curve in Fig. 5A is the least-square fit using one-step kinetics model (shown only for the purpose of comparison), and that in Fig. 5B is the best fit using two-step kinetics model. It is obvious that the two-step model displays better numerical approximation to the experimental event. Kinetic parameters for the second group of curves are also given in Table 1.

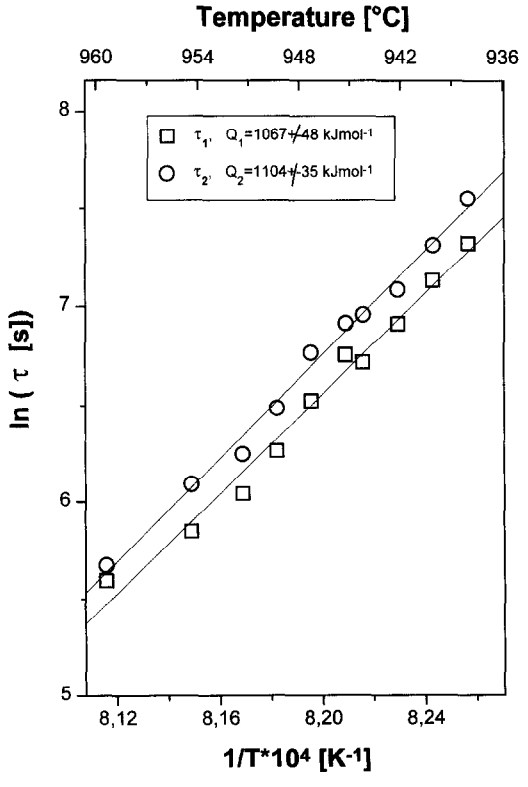

Fig. 6. Arrhenius plot of incubation times $\ln \tau_1$ and $\ln \tau_2$ versus $1/T$. $\ln \tau_1 = 128360.61(1/T) - 98.7$; linear regression; correlation factor $R_1 = 0.992$; $\Rightarrow Q_1 = 1067 \pm 48$ kJ mol^{-1}. $\ln \tau_2 = 132826.66(1/T) - 102.16$; linear regression; correlation factor $R_2 = 0.996$; $\Rightarrow Q_2 = 1104 \pm 35$ kJ mol^{-1}.

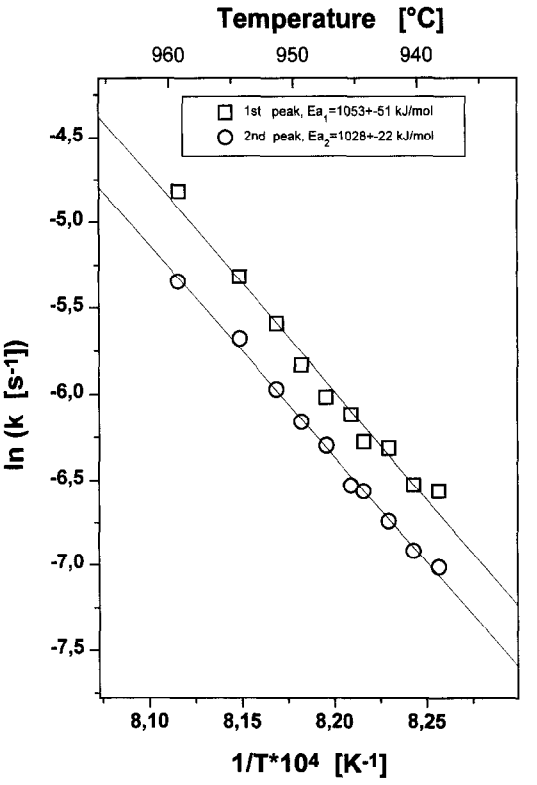

Fig. 7. Arrhenius plot of $\ln k$ vs. $1/T$ (rate constants k_1 and k_2 from Table 1). For the first step of crystallization: $\ln k_1 = -126704.83(1/T) + 97.92$; linear regression; correlation factor $R_1 = 0.991$; $\Rightarrow E_{a1} = 1053 \pm 51$ kJ mol^{-1}. For the second step of crystallization: $\ln k_2 = -123679.74\ (1/T) + 95.05$; linear regression; correlation factor $R_2 = 0.998$; $\Rightarrow E_{a2} = 1028 \pm 22$ kJ mol^{-1}.

$(\Delta H)_T$ in Table 1 is the reaction enthalpy for the whole process and is given per mole of the sample left after DSC analysis. The τ_1 and τ_2 are real incubation times. By taking experimental errors into account, the Avrami exponents n_1 and n_2 are assumed constant and equal for different annealing temperatures, implying that the nucleation and growth are independent of temperature. Both rate constants, k_1 and k_2, are functions of temperature, as expected, and increase with the annealing temperature. They are assumed to follow Arrhenius dependence: $k =$

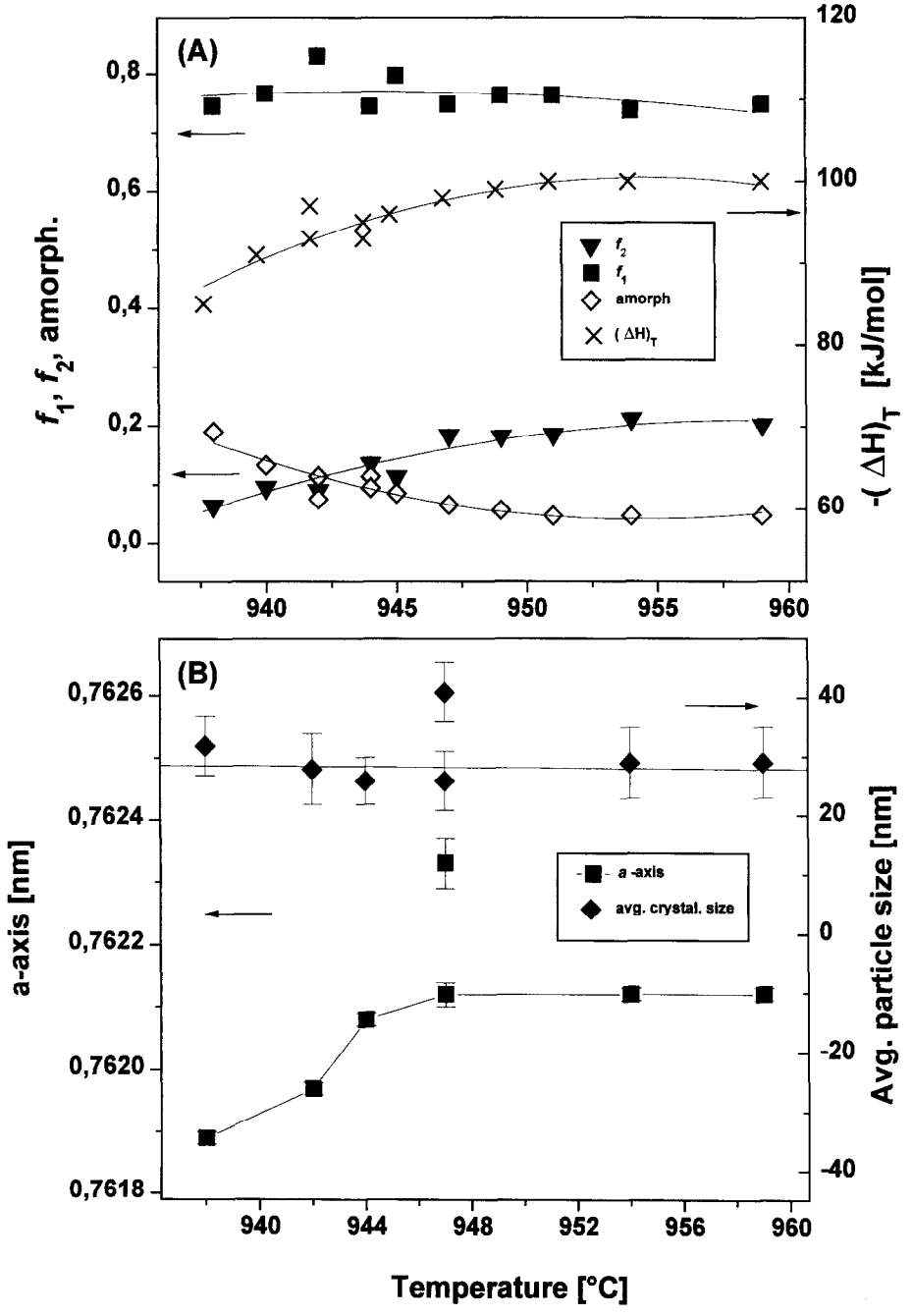

Fig. 8. (A) Mullite fraction, calculated from DSC scan under assumption of two-step crystallization kinetics, vs. annealing temperature. f_1 = fraction of mullite formed in the first step, f_2 = fraction of mullite formed in the second step of mullitization, ◇ = amorphous phase, × = reaction enthalpy, $(\Delta H)_T$. (B) Mullite a-axis length and average particles size vs. annealing temperature. Lines are drawn as guides for the eye.

$k_0 \exp(-E_a/RT)$. E_a is the activation energy for crystallization.

The calculated values of τ_1 and τ_2 are plotted vs. transformation temperature as an Arrhenius plot in Fig. 6. From the slope of plots $\ln \tau_1$ and $\ln \tau_2$ vs. $1/T$, activation energies for incubation: $Q_1 = 1067 \pm 48$ kJ mol^{-1}, and $Q_2 = 1104 \pm 35$ kJ mol^{-1} can be derived [21]. Arrhenius plots of rate constants, k_1 and k_2, fitted on the basis of least-squares regression are shown in Fig. 7. From the slope of straight lines, apparent activation energies of mullite crystallization are derived. The values of $E_{a1} = 1053 \pm 51$ kJ mol^{-1} and $E_{a2} = 1028 \pm 22$ kJ mol^{-1} were obtained.

Fraction of mullite crystallized at the completion of the process, w, depends on annealing temperature, and can be determined using the expression $w = (\Delta H)_T/(\Delta H)_c$. Taking into consideration that mullite is the sole crystalline phase in the system (Fig. 4), and that the crystallization of the same fraction of mullite is expected to be related to the same enthalpy release, as well as that there is no significant difference between activation energies for both individual processes, the following relations should be valid: $f_1 = Aw$ and $f_2 = (1 - A)w$, and $f_1 + f_2 + A_m = 1$, where f_1 is the fraction of mullite formed in the first step and f_2 in the second step of crystallization, respectively, and A_m is the untransformed amorphous part of the sample. The values of f_1, f_2 and A_m as a function of annealing temperature are shown in Fig. 8A. Mullite crystallizing in the first step increases with annealing temperature to the limit of $f_1 \approx 0.20$ on the account of amorphous phase, whereas f_2 is almost constant in the whole temperature range. Annealing above 947°C does not bring any changes in mullite fractions, or in the reaction enthalpy, $(\Delta H)_T$, as also shown in Fig. 8A.

Mullite lattice constants were determined by Rietveld refining method [12,13]. The refinement was performed iteratively, starting with an average mullite structure as an initial model. Occupation factors were set to values derived from x-values according to the formula of mullite solid solution ($Al_{4+2x}Si_{2-2x}O_{10-x}$). The refinement was repeated until the best fit was obtained. Lattice constants, and amount of Al_2O_3 in mullite (derived from the relation: Al_2O_3 [mol%] = $1443a - 1028.06$) [14], as well as the average particle size evaluated from XRD line broadening are listed in Table 2. The length of mullite a-axis and average crystal size as a function of annealing temperature are given in Fig. 8B. The a-axis length increases with annealing temperature to a maximum of $a = 0.76212(2)$ nm at 947°C, corresponding to 72.0 mol% of Al_2O_3 in mullite. Above 947°C there were no detectable changes in the a-axis, consequently, no significant changes in mullite composition, occurred. There is no difference in average mullite crystallite size throughout the temperature range. This uniformity is in accordance to the data obtained by Li and Thomson [6]. Mullite a-axis length and primary particle size for the sample annealed at 947°C and quenched immediately after the first DSC peak had been achieved are also given in Fig. 8B. Mullite exhibited greater a-axis. It is an additional confirmation that mullite with greater alu-

Table 2
Mullite lattice constants from Rietveld refinement, Al_2O_3 content, and mullite particle size

T (°C)	Mullite (nm)			Al_2O_3 [a] (mol%)	Average particle size [b] (nm)
	a	b	c		
938	0.76189(1) [c]	0.76767(1)	0.288609(2)	71.4	32 ± 5
942	0.76197(1)	0.76721(1)	0.288600(2)	71.5	28 ± 6
944	0.76208(1)	0.76767(1)	0.288780(2)	71.6	26 ± 4
947	0.76212(2)	0.76721(2)	0.288690(2)	71.7	26 ± 5
947	0.76233(4) [d]	0.76954(3)	0.28891(1)	72.0	41 ± 5
954	0.76212(1)	0.76720(2)	0.288617(1)	72.0	29 ± 6
959	0.76212(1)	0.76723(1)	0.288450(1)	72.0	29 ± 6

[a] Calculated from the relation: Al_2O_3 [mol%] = $1443a - 1028.06$ (a-axis length) given by Ban and Okada [14].
[b] Mean calculated value using 13 strong reflections in a diffraction angle interval of 30–70° 2θ.
[c] Number in parentheses correspond to std. dev. for last place quoted.
[d] Sample was quenched and analysed subsequently after the first peak on DSC was achieved.

mina content crystallizes first. More comprehensive data are needed to answer whether the larger crystallite size measured in the same specimen is also characteristic of the first-step process.

4. Discussion

Non-isothermal DSC analysis of the as-dried gel (Fig. 1) shows that gel crystallization occurs during a single exothermic peak at 983.5°C. The peak can be attributed to formation of mullite, or spinel, or both. A broader and smaller exotherm, followed by an additional exothermic peak at 1250°C is characteristic of Al–Si spinel [4]. In Fig. 1A inset (2), the peak corresponding to spinel transformation is not detected. XRD analyses (Fig. 4) confirmed that gel derived from ANN and TEOS can be termed 'single phase', because it transforms directly to mullite without forming Al–Si spinel. The crystallization enthalpy determined from the integral of the DSC maximum at 983.5°C $(\Delta H)_c = -105$ kJ mol^{-1} is in agreement with the value $(\Delta H)_c = -106$ kJ mol^{-1} obtained by Sen and Thiagarajan [18]. Since duplicate runs of crystallization enthalpy measurements (at the beginning and at the end of this study) were in excellent agreement, we assumed that as-dried gel is homogeneous prior to heating. Therefore, two overlapping peaks seen in isothermal DSC curves above 947°C (Fig. 2C), are attributed to a property of the gel and not to changes in the gel structure during storage. Moreover, the changes in gel structure should become apparent in DSC scans at low temperature, which was not the case.

While crystallization of mullite under non-isothermal conditions was observed in one DSC exotherm, the crystallization of mullite under isothermal conditions had one DSC exotherm below, and two overlapped exothermic peaks above 947°C. These maxima indicate that mechanisms of mullite crystallization below 947°C differ from those above. However, the DSC data even below 947°C do not fit the one-step model well (Fig. 3A). Therefore, a bimodal kinetic model (Eq. (1)) was applied even for DSC data with one exotherm. The same bimodal or two-step model was also applied for data with two overlapped exotherms (annealing temperatures above 947°C). According to the data shown in Table 1 and in Fig. 3B and Fig. 5B, a two-step crystallization model fits experimental data within $\pm 2\%$ in the whole temperature range. That means, two transformation processes follow one after another with a small time lag. The higher the annealing temperature, the smaller the time lag between these two processes, and at $T \approx 959.8$°C (extrapolated value) they should start simultaneously. Whereas, mullite fraction transformed during the first step, f_1, is small and varies with annealing temperature, most of the mullite, f_2, crystallizes in the second step, and is independent of temperature (Fig. 8). The same apparent activation energies can be assumed for both processes, since the difference between $Ea_1 = 1053 \pm 51$ kJ mol^{-1} and $E_{a2} = 1028 \pm 22$ kJ mol^{-1} lies in the range of the measurement's accuracies (Fig. 7). Furthermore, the processes of growing mullite grains are similar to the processes of mullite nucleation (activation energies for incubation are: $Q_1 = 1067 \pm 48$ kJ mol^{-1} and $Q_2 = 1104 \pm 35$ kJ mol^{-1}).

The time exponent, n, varies from 3.06 to 3.52 for the first process and from 3.05 to 3.52 for the second one. The means, $n_1 = 3.37$ and $n_2 = 3.45$ do not determine the process mechanism with certainty. Since mullite particle size is almost independent of annealing temperature (Fig. 8B), a nucleation-controlled mechanism could be assumed for both steps of crystallization [6].

Two-step nucleation-controlled process of mullite crystallization in single-phase gels, was also proposed by Li and Thomson [6]. However, there is a discrepancy between the results found in this work and those determined by Li and Thomson. They determined one order of magnitude larger rate constants, and the apparent activation energies were $Ea_1 = 263 \pm 145$ kJ mol^{-1} and $Ea_2 = 362 \pm 145$ kJ mol^{-1}. On the other hand, apparent activation energies evaluated by Wei and Halloran [7,8] for diphasic ($Ea = 1070 \pm 200$ kJ mol^{-1}) and by Huling and Messing [22] for hybrid gels ($Ea = 1091 \pm 71$ kJ mol^{-1}) reveal a consistency with those of ours, although there is a difference in the temperature of transformation (> 200°C). The kinetics data are not sufficient to determine if the process is a typical single phase one (nucleation-controlled process with two rate constants and small apparent activation energies), or a hybrid gel one (mullite formation via spinel and high apparent activation energies).

Huling and Messing [22] found that the process conditions favouring alumina segregation and spinel nucleation are the factors controlling transformation kinetics of hybrid (and colloidal) gels. Further, they assumed that nanometer-scaled alumina regions can occur also in any single phase gel. Mixing colloidal gel with a single-phase (as Huling and Messing prepared hybrid gels) enabled formation of boehmite in situ, which then acted as a nucleus for spinel. In the as-prepared single-phase gel (dried at 60°C) alumina component is preferentially present as nitrate in a branched polymeric silica network [5,23]. Therefore, alumina dispersion through silica network is much finer than that assumed for boehmite in hybrid gels. On the other hand, sample storage in desiccator and rapid heating to annealing temperature did not allow boehmite formation (or any crystalline form of alumina).

Since a two-step model describes all experimental data with satisfaction, there is a question how to explain crystallization of one phase by two exothermic processes. Huling and Messing [9] were the first who reported low temperature mullite formation in single-phase gels. Ban et al. [16] found low temperature formation to occur only when as-prepared gel was heated at 250°C for some time. The heated precursor showed two-step formation; small amount of mullite was formed at 450°C, whereas most of the mullite crystallized at 900°C. The as-prepared precursor showed only one-step formation at around 900°C. The authors [16] explained the two-step formation by existence of small regions with differing compositions within the precursor particles. The interface areas between them acted as heterogeneous nucleation sites for first-step formation. This interpretation could be accepted to explain two overlapped peaks seen in the isothermal DSC scan above 947°C. However, it does not explain why the amount of mullite derived from interfacial areas (which is supposed to be identical to f_1 in our study) increases with annealing temperature to 947°C and above remains constant.

Using the relationship between a-axis length and alumina content in mullite (Al_2O_3[mol%] = $1443a - 1028.06$) [14] it could be possible to distinguish mullites that crystallize from the proposed different regions. Unfortunately, these two processes occur in an overlapping temperature range, as shown by kinetic analysis. Therefore, information on the separate mullite composition for each of these processes, is not available. Only an integral composition can be obtained. Nevertheless, from the change of the mullite a-axis length with temperature (shown in Fig. 8B), compared with the mullite fraction formed in the first and second step (f_1, and f_2) (Fig. 8A), an estimation of composition of these two mullites was made. Mullite that crystallizes in the first process consumes alumina-richer amorphous phase, whereas mullite that crystallizes in the second process matches more closely the original homogeneous gel. By increasing the amount of alumina-richer mullite, f_1, the alumina content in the average mullite composition also increases, reaching the highest point at 947°C and from then on remaining stable. The mullite fraction crystallized in the second step, f_2, is nearly constant and independent of temperature. At 947°C, an equilibrium between f_1 and f_2 is attained.

To understand these results, the process occurring prior to mullite crystallization at 980°C has to be considered as an operative mechanism that governs the crystallization of mullite in two steps. Two separated exothermic peaks at about 980°C in dynamic DTA data of precursors prepared by CVD have been observed by Gani and McPherson [24], and Hori and Kurita [25]. They found that both peaks correspond to mullite crystallization, and have attributed them to a metastable liquid immiscibility in the Al_2O_3-rich region of Al_2O_3–SiO_2 binary system. Huling and Messing [9] recently have attributed the crystallization of Al-rich mullite rather than stoichiometric mullite in homogeneous single-phase gels at 980°C to phase separation. They found that, by suppressing the phase separation, the gels crystallize directly to orthorhombic mullite at temperatures as low as 700°C. The localized compositional changes involved in phase separation preclude formation of stoichiometric mullite in favour of metastable alumina-rich form. Rapid heating is insufficient to prevent phase separation. Instead, there must be some aspect of a gel's aging process that slows phase separation relative to crystallization. Furthermore, they observed an interconnected two-phase morphology on TEM micrographs of amorphous gel-flakes heat treated at 900°C. Interconnected two-phase morphology is characteristic of phase separated material and is generally attributed to a spinodal phase sepa-

ration mechanism [26]. MacKenzie et al. [27] have also found that the evolution of mullite at 980°C is affected by thermal treatment of mullite precursors at lower temperatures. They assumed that thermal treatment induces formation of phase separated microdomains or oxygen deficient Al-triclusters, which are responsible for Al-rich mullite crystallization at 980°C. They also pointed out that phase separation should be much weaker in single-phase gels than in diphasic precursors, from which mullite and spinel crystallize at 980°C. If the formation of Al-rich mullite and amorphous SiO_2 phase, on the one hand, and mullite and Al–Si spinel, on the other hand, are attributed to phase separation, then phase separation can also be assumed to precede the crystallization in our single phase gel. An interconnected two-phase morphology similar to the one observed by Huling and Messing [9] was determined also by us in an amorphous gel-foil [17] prepared from the identical wet gel, as the one used in this study. Since all specimens were heated in the same way to an annealing temperature, the same degree of phase separation could be expected. As our study showed, we measured a constant $(f_1 + A_m)/f_2$ ratio for each of the annealing temperatures (Fig. 8A), which confirms this expectation. The question that arises from these results is whether another heating rate would change the $(f_1 + A_m)/f_2$ ratio. Our preliminary experiments have shown that the heating rate affects the $(f_1 + A_m)/f_2$ ratio. Simultaneous DTA/TG and MS analyses of different treated single-phase mullite gels correlated with the ratio of f_1/f_2 might give an answer to the question of how to suppress the processes involved in phase separation. Further work is needed to clarify these questions.

We conclude that, under applied experimental conditions (heating rate of 30 K/min), phase separation proceeds more rapidly than crystallization, reducing the high free energy of the homogeneous amorphous system. In addition, phase separation determines the mass ratio of the two mullites. This effect implies that crystallization of mullite at 980°C in two steps is not only a matter of nucleation and growth limitations but is also controlled by phase separation.

The described kinetics analysis permitted more direct insight into the reaction of mullite formation from single-phase gels.

5. Conclusion

There are two processes with different rates which occur successively with a small time lag. A two-step model was used to evaluate the kinetic parameters satisfactorily. The magnitude of the ns gave no reliable information about the crystallization mechanisms.

The apparent activation energies ($E_{a1} = 1053 \pm 51$ kJ/mol, and $E_{a2} = 1028 \pm 22$ kJ mol^{-1} for both processes are much greater than those for single phase gels reported in the literature.

Phase separation has to be assumed to describe our results satisfactorily.

The thermal treatment regime to bring the gels to crystallization temperature affects phase separation, and consequently the crystallization mechanism of this aluminosilicate system.

References

[1] K. Okada, N. Otsuka, S. Somiya, Am. Ceram. Soc. Bull. 70 (1991) 1633.

[2] D.W. Hoffmann, R. Roy, S. Komarneni, J. Am. Ceram. Soc. 67 (1984) 468.

[3] K. Okada, N. Ôtsuka, in: S. Somiya, R.F. Davis, J.A. Pask (Eds.), Ceramic Transactions, Vol. 6, Mullite and Mullite Matrix Composites, American Ceramic Society, Westerville, OH, 1990, p. 375.

[4] H. Schneider, K. Okada, J. Pask, Mullite and Mullite Ceramics, Wiley, Chichester, 1994, p. 105.

[5] K. Okada, C. Aoki, T. Ban, S. Hayashi, A. Yasumori, J. Eur. Ceram. Soc. 16 (2) (1996) 149.

[6] D.X. Li, W.J. Thomson, J. Am. Ceram. Soc. 73 (1990) 964.

[7] W.-Ch. Wei, J.W. Halloran, J. Am. Ceram. Soc. 71 (1988) 166.

[8] W.-Ch. Wei, J.W. Halloran, J. Am. Ceram. Soc. 71 (1988) 581.

[9] J.C. Huling, G.L. Messing, J. Non-Cryst. Solids 147&148 (1992) 213.

[10] D.X. Li, W.J. Thomson, J. Mater. Res. 5 (1990) 1963.

[11] I.W. Donald, J. Mater. Sci. 30 (1995) 904.

[12] H.M. Rietveld, J. Appl. Crystallogr. 2 (1969) 65.

[13] M. Schneider, Software Package for Rietveld Analysis of X-ray and Neutron Diffraction Patterns, Wyriet, version 3.

[14] T. Ban, K. Okada, J. Am. Ceram. Soc. 75 (1992) 227.

[15] A. Brown, J.W. Edmonds, Adv. X-Ray Anal. 23 (1980) 361.

[16] T. Ban, S. Hayashi, A. Yasomuri, K. Okada, J. Eur. Ceram. Soc. 16 (1996) 127.

[17] R. Nass, E. Tkalcec, H. Ivankovic, J. Am. Ceram. Soc. 78 (1995) 3097.

[18] S. Sen, S. Thiagarajan, Ceram. Int. 14 (1988) 77.

[19] J.W. Christian, The Theory of Transformations in Metals and Alloys, 2nd ed., Pergamon, Oxford, 1975.

[20] S. Kurajica, A. Bezjak, E. Tkalcec, Resolving overlapping peaks and determination of kinetic parameters for crystallization of multicomponent system from DTA or DSC curves, II. Isothermal kinetics, Thermochim. Acta, in press.
[21] B.O. Hildmann, H. Schneider, M. Schmücker, J. Eur. Ceram. Soc. 16 (1996) 287.
[22] J.C. Huling, G.L. Messing, J. Am. Ceram. Soc. 74 (1991) 2374.
[23] M. Fukuoka, Y. Onoda, S. Inoue, K. Wada, A. Nukui, J. Sol–Gel Sci. Technol. 1 (1993) 47.
[24] M.S.J. Gani, R. McPherson, J. Mater. Sci. 12 (1977) 999.
[25] S. Hori, R. Kurita, in: S. Somiya, R.F. Davis, J.A. Pask (Eds.), Ceramic Transactions, Vol. 6, Mullite and Mullite Matrix Composites, American Ceramic Society, Westerville, OH, 1990, p. 311.
[26] C.M. Jansen, D. Schwahn, J. Schelte, H. Herman, Phys. Chem. Glasses 22 (1981) 122.
[27] MacKenzie, R.H. Meinhold, J.P. Patterson, H. Schneider, M. Schmücker, D. Voll, J. Eur. Ceram. Soc. 16 (1996) 1299.